Plasmonic band-stop filter with asymmetric rectangular ring for WDM networks

2013 J. Opt. 15 055007

(http://iopscience.iop.org/2040-8986/15/5/055007)

IOP Publishing Journal of Optics
J. Opt. **15** (2013) 055007 (7pp) doi:10.1088/2040-8978/15/5/055007

Plasmonic band-stop filter with asymmetric rectangular ring for WDM networks

Vahid Foroughi Nezhad[1], **Siamak Abaslou**[2] **and Mohammad Sadegh Abrishamian**[1]

[1] Department of Electrical Engineering, K N Toosi University of Technology, PO Box 16315-1355, Tehran, Iran
[2] Department of Electrical and Computer Engineering, Rutgers University, Piscataway, NJ 08854, USA

E-mail: foroughi.vahid@ee.kntu.ac.ir, s.abaslou@rutgers.edu and msabrish@eetd.kntu.ac.ir

Received 6 November 2012, accepted for publication 8 March 2013
Published 11 April 2013
Online at stacks.iop.org/JOpt/15/055007

Abstract
We proposed a simple asymmetric rectangular band-stop filter based on metal–insulator–metal plasmonic waveguides. It is shown that the performance of the structure as a filter strongly depends on the asymmetry of the rectangular structure. An analytical model based on the analogy between MDM waveguides and the microwave transmission line is used to calculate the resonance wavelengths and explain the behavior of the filter. The bandwidth of spectra can be easily manipulated by adjusting the topological parameters of the filter. It is also demonstrated that by adjusting the bandwidth, the filter can be used for CWDM standard channels. The filter behavior is verified using the numerical finite difference time domain (FDTD) method. The filter is compact and has a footprint of 1 μm $\times$ 0.5 μm, which is suitable for integrated optical circuits.

Keywords: plasmonics, surface plasmon polaritons, MIM waveguide, plasmonic filter, ring resonator

(Some figures may appear in colour only in the online journal)

1. Introduction

Surface plasmon polaritons (SPPs) are considered as the most promising way for the realization of highly integrated optical circuits due to their capability to overcome the diffraction limit of light [1, 2]. Among various SPP structures [3], the metal–insulator–metal (MIM) structure [4, 5] has attracted great interest from researchers in recent years, because of its potential applications to manipulate and control light on the nanoscale. Various passive MIM waveguide components have been demonstrated by numerical simulation and experiment, such as couplers [6], splitters [7, 8], Mach–Zehnder interferometers and ring resonators [9, 10]. The development of other plasmonic devices, such as band-pass or band-stop filters, may be necessary to fabricate high-density integrated optical circuits. So far, various kinds of plasmonic filters based on metal–insulator–metal (MIM) structures have been proposed. In this regard, plasmonic filters based on circular rings [11, 12], rectangular rings [13–15], slot cavities [16–19], nano-capillary resonators [20] and stub structures [21–28] have been investigated. A plasmonic infrared filter by localized surface plasmon polaritons in a $Ag/SiO_2/Ag$ T-shaped array was theoretically and experimentally investigated [29]. In conventional band-stop filters, the ring resonator is separated from the bus waveguide by a gap, which is generally about 25 nm, to keep efficient coupling; however, in practice, realizing this gap may not be easily achievable. So far some gapless structures based on the aperture-coupled device using circular ring and cavity slot resonators have been proposed to overcome this problem [30, 31]. In this paper an easy-to-fabricate novel and simple plasmonic band-stop filter composed of an asymmetric

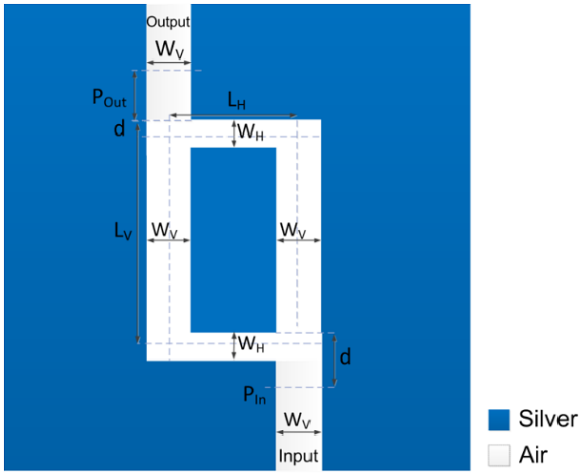

Figure 1. Schematic diagram of an asymmetric rectangular band-stop filter.

rectangular ring which has the advantage of being gapless and aperture-coupled is proposed. The finite difference time domain (FDTD) method is used as a numerical method to simulate the structures. Also, a circuit model based on transmission line theory is proposed to characterize the behavior of the filter. We focus on the design of a filter for optical communication wavelengths and study its tunability by changing the structural parameters. It is shown by choosing appropriate parameters that the filter can be used as a tunable filter in CWDM networks.

The schematic of an asymmetric band-stop rectangular filter is shown in figure 1. It is composed of an asymmetric rectangular ring between two waveguides acting as input and output ports in the structure. The materials used in this filter are air $\varepsilon_d = 1$ and silver, whose complex relative permittivity is characterized by the Drude model: $\varepsilon_m(\omega) = \varepsilon_\infty - \omega_p^2/\omega(\omega + i\gamma)$, where $(\varepsilon_\infty, \omega_p, \gamma) = (3.7, 9.1, 0.018\ \text{eV})$ [28]. The structure is studied in two dimensions due to its infinitely long aspect in the direction normal to the paper. Due to the small size of the widths of the waveguides it is assumed that only the fundamental mode, TM_0, can propagate in the MIM waveguides. The complex propagation factor β can be obtained by solving the following dispersion relation equation [32]:

$$\tanh\left(\frac{K_d}{2}w\right) = -\frac{\varepsilon_m K_m}{\varepsilon_d K_d} \tag{1}$$

where ε_d and ε_m correspond to the dielectric constant of the insulator and the metal respectively. K_i $(i = d, m)$ is the wavenumber component, perpendicular to the interface in two media, defined as

$$K_d = \left(\beta^2 - \varepsilon_d K_0^2\right)^{1/2}, \qquad K_m = \left(\beta^2 - \varepsilon_m K_0^2\right)^{1/2} \tag{2}$$

where $K_0 = 2\pi/\lambda$ is the wavenumber of the wave propagating in vacuum.

2. Theoretical background

The structure shown in figure 1 acts as a band-stop filter which prohibits propagation of light at some wavelengths. By using

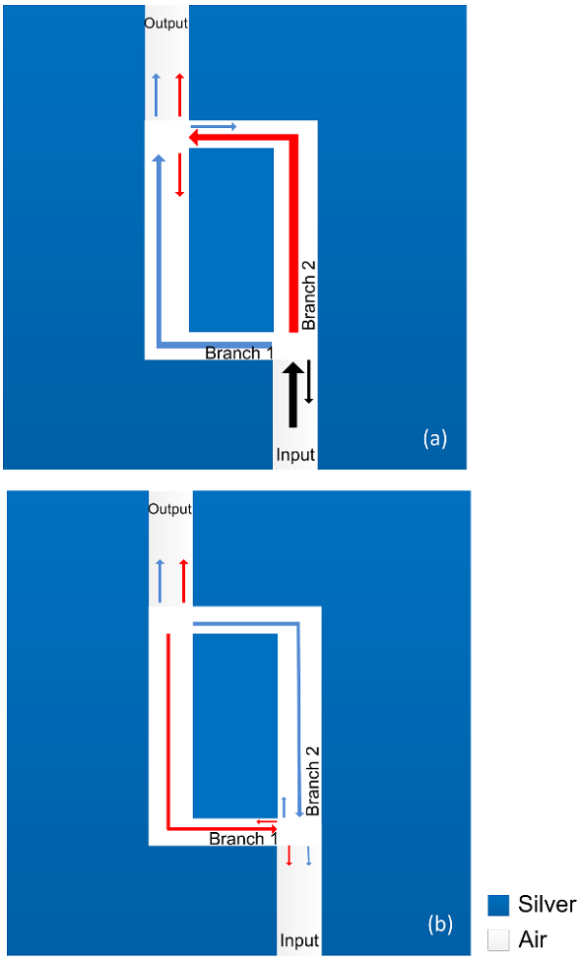

Figure 2. (a) The first and second splitting of the light at the input and output junctions. (b) The third splitting of the light at the input junction.

an asymmetric ring as a resonator of the filter, stable standing waves can be excited at some specific wavelengths and the light cannot pass at these wavelengths. Asymmetry in the structure shown in figure 1 is caused by three factors: first, the difference between the vertical and horizontal length of the waveguides $L_H \neq L_V$; second, the difference between the vertical and horizontal width of the waveguides $W_H \neq W_V$; and third, the asymmetry in location of the input and output ports. For a symmetric structure the input and output ports are located in the middle of the horizontal branches. In the structure shown, the input and output ports are located at right and left corners respectively. Here, the locations of the input and output ports are set to be fixed because it will be shown that by adjusting the first and second aforementioned factors we can completely control the behavior of the filter.

To analyze the behavior of the filter qualitatively, as demonstrated in figure 2(a) at a given wavelength, the light emitted from the input port encounters the input junction and, according to the impedances of each branch, it splits into three beams: one beam is reflected and two beams enter the ring. Both of the beams entering the ring experience another splitting process at the output junction as they propagate in the ring. At the output junction both of these beams split into

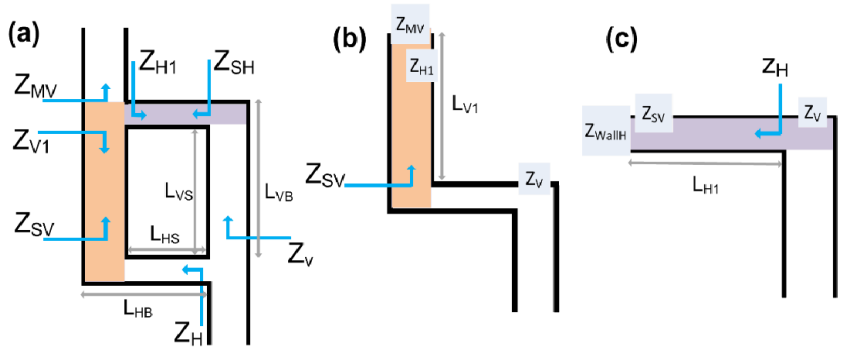

Figure 3. The steps for calculating Z_H.

two new beams: one of these new beams enters the output port and the other beam propagates in the other branch and stays in the ring. The beams staying in the ring propagate towards the input junction and again both beams experience another splitting process at the input junction. As seen from figure 2(b), two beams stay in the ring. The beams staying in the ring are responsible for standing waves excited inside the ring. The process of splitting at the input and output junctions happens countless times for each of the two beams staying in the ring, which propagate clockwise and counterclockwise respectively. If the wavelength of the light is one of the resonance wavelengths then each beam will form a standing wave. The standing waves at resonance wavelengths have minimum intensities at the input and output ports. In other words, the beams exciting the stable standing waves in the ring are applied from the notch point of the stable standing waves in the ring. Knowing this fact and according to direction of propagation, the standing waves excited by each of the two beams have a π radian phase shift. Therefore when the two beams staying in the ring, propagating clockwise and counterclockwise, are equal or the structure is completely symmetric, the light cannot excite any stable standing wave in the ring. However, when the structure is asymmetric these two beams will not be equal, thus the light is capable of exciting stable standing waves at some specific wavelengths. After reaching a stable state at the resonance wavelengths the light at these wavelengths cannot exit the structure, because the output port is located at the notch point of the stable standing waves [18].

3. Analytical model

As has been discussed, the performance of the structure as a filter is based on the difference between the impedances seen from each branch of the ring at the input junction, (Z_H and Z_V demonstrated in figure 3(a)). To calculate these impedances the analogy between the subwavelength waveguides in photonics and transmission lines in microwaves is used [14, 24–26, 33, 34]. Applying this analogy, all the MDM waveguides in the structure can be replaced by the equivalent transmission lines demonstrated in figure 3(a), the characteristic impedances of which can be obtained using the following relation [26]:

$$z_{\mathrm{MDM}} = \frac{wE_y}{H_z} = \frac{w\beta(w)}{\omega\varepsilon_0\varepsilon_d} \tag{3}$$

where W is the width of the waveguide, β is the propagation constant of the fundamental mode of the waveguide, which can be obtained by solving equations (1) and (2), and ε_d is the permittivity of the dielectric. To calculate Z_H and Z_V, one can use equations (4) and (5). The parameters used in these equations are listed in the table 1. It is seen from figure 3(c), that to calculate Z_H, Z_{WallH} and Z_{SV} should be defined first. Based on [26], the parameter Z_{WallH} shown in figure 3(c) is defined as $Z_{WallH} = \sqrt{\varepsilon_d/\varepsilon_m} z_{MH}$, where ε_m is the frequency-dependent complex dielectric constant of silver. The other parameter needed to be calculated is Z_{SV}. Based on figure 3(b) to calculate Z_{SV} we need to know Z_{H1} and, due to symmetry of the structure shown in figure 3(a), one can construe $Z_H = Z_{H1}$, $Z_V = Z_{V1}$; therefore by using equation (4) and utilizing iteration, Z_H can be easily calculated. The steps for calculating Z_V are similar to the steps for calculating Z_H.

$$Z^N_{LH1} = Z^N_H + Z_{MV} \tag{4a}$$

$$Z^N_{SV} = Z_{MV} \times \frac{(Z^N_{LH1} - iZ_{MV}\tan(\beta_V L_{V1}))}{(Z_{MV} - iZ^N_{LH1}\tan(\beta_V L_{V1}))} \tag{4b}$$

$$Z^N_{LH2} = Z^N_{SV} + Z_{WallH} \tag{4c}$$

$$Z^{N+1}_H = Z_{MH} \times \frac{(Z^N_{LH2} - iZ_{MH}\tan(\beta_H L_{H1}))}{(Z_{MH} - iZ^N_{LH2}\tan(\beta_H L_{H1}))} \tag{4d}$$

$$Z^N_{LV1} = Z^N_V + Z_{MV} + Z_{WallH} \tag{5a}$$

$$Z^N_{SH} = Z_{MH} \times \frac{(Z^N_{LV1} - iZ_{MH}\tan(\beta_H L_{H1}))}{(Z_{MH} - iZ^N_{LV1}\tan(\beta_H L_{H1}))} \tag{5b}$$

$$Z^N_{LV2} = Z^N_{SH} + Z_{WallV} \tag{5c}$$

$$Z^{N+1}_V = Z_{MV} \times \frac{(Z^N_{LV2} - iZ_{MV}\tan(\beta_V L_{V1}))}{(Z_{MV} - iZ^N_{LV2}\tan(\beta_V L_{V1}))}. \tag{5d}$$

In equations (4) and (5), N specifies the number of iterations. Initial values of Z_H and Z_V are set to be zero. The values of these two impedances for a filter with parameters of $W_H = 40$ nm, $W_V = 100$ nm, $L_H = 200$ nm, and $L_V = 500$ nm after 50 iterations are calculated and, after being divided

Table 1. The list of parameters used in equations (4) and (5).

Parameter	Definition
$L_{H1} = L_H - W_V/2$	The average of $L_{HS} = L_H - W_V$ and $L_{HB} = L_H$
$L_{V1} = L_V - W_H/2$	The average of $L_{VS} = L_V - W_H$ and $L_{VB} = L_V$
Z_{MH}, Z_{MV}	Characteristic impedances of waveguides with widths W_H and W_V respectively
Z_{WallH}, Z_{WallV}	Impedances of the wall of waveguides with widths W_H and W_V respectively
β_H, β_V	Propagation constants of the waveguides W_H and W_V respectively
Z_{H1}, Z_{V1}	Impedances of the branches seen from the output junction
Z_{SV}, Z_{SH}	The impedance seen from the left and right corners respectively, as shown in figure 3(a)
Z_{LH1}, Z_{LH2}, Z_{LV1}, Z_{LV2}	These four parameters are defined in the equations and used to simplify the calculation process

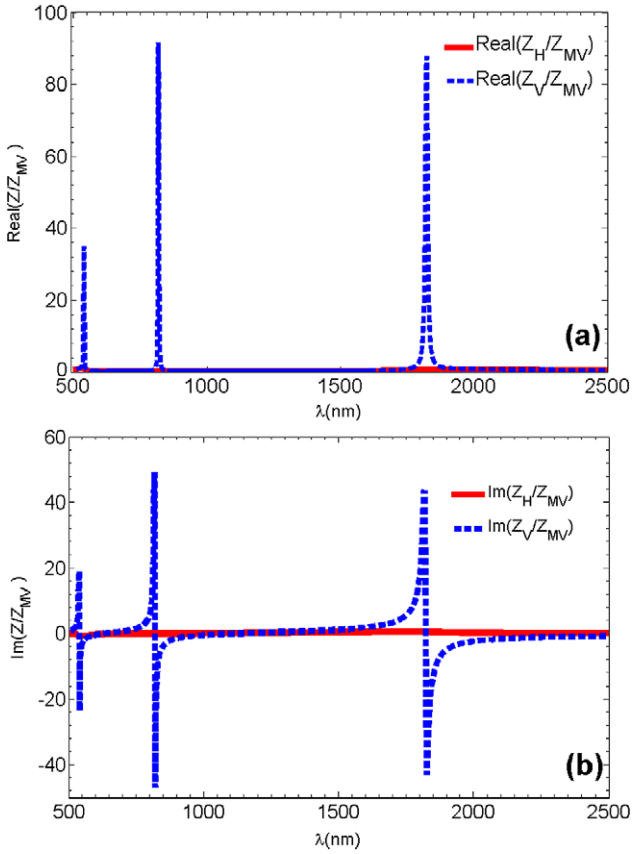

Figure 4. The values of Z_V/Z_{MV} and Z_V/Z_{MV} after 50 iterations. (a) Real parts of Z_V/Z_{MV} and Z_H/Z_{MV}. (b) Imaginary parts of Z_V/Z_{MV} and Z_H/Z_{MV}.

by characteristic impedance of the waveguide (Z_{MV}), are shown in figure 4. Figure 4(a) shows the real part of Z_H/Z_{MV} and Z_V/Z_{MV} and figure 4(b) shows the imaginary parts of these ratios. As has been explained, the resonant wavelength occurs where the difference between Z_H and Z_V becomes maximum; therefore by calculating Z_H and Z_V we can find the resonance wavelengths. In figure 4, the wavelengths at which the difference between Z_H/Z_{MV} and Z_V/Z_{MV} is maximum are in fact the resonance wavelengths.

We propose a model based on the difference between Z_H and Z_V. The basic principle is that the system should work as a filter when Z_H and Z_V are different, whereas when $Z_H = Z_V$ there should be no filtering and the general form of

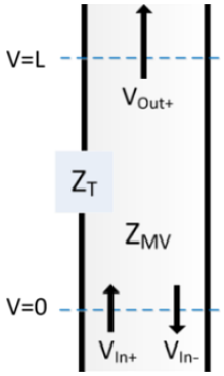

Figure 5. The equivalent transmission line model representation of the filter.

the impedance which can be used as an analytic model for the structure would be $Z_T = A(\lambda)\,|(Z_V - Z_H)|^X$, where $A(\lambda)$ is a coefficient, which in general form is a function of wavelength, and X is a positive real number. Our proposed model is $Z_T = 5\,|Z_H - Z_V|^{1.3}$. For simplicity, it is assumed that $X = 1.3$ and $A(\lambda) = 5$. It will be shown that this simplified model, as well as being useful for calculating the resonance wavelengths, can be used to explain the behavior of the filter. Transmission spectra of the simplified model shown in figure 5 can be easily obtained using the transfer matrix method [25].

$$T = \left|\frac{V_{Out+}}{V_{In+}}\right|^2 = \left|\left(1 + \frac{Z_T}{2Z_{MV}}\right)\right|^{-2} e^{\left(\frac{-L}{L_{SSPY}}\right)} \qquad (6)$$

where $L_{SSPY} = |2\mathrm{Im}(\beta_V)|^{-1}$ and β_V are the propagation length and propagation constant of the waveguides with width of W_V, and $L = 2d$ and d is the distance between sampling lines and junctions in figure 1. In order to consider the loss effect for traveling waves in the ring, the transmission calculated using equation (6) should be multiplied by $e^{\left(-\frac{L_H}{L_{SSPH}} - \frac{L_V}{L_{SSPV}}\right)}$, where $L_{SSPH} = |2\mathrm{Im}(\beta_H)|^{-1}$ is the propagation length of the waveguides with a width of W_H.

4. Results

For simulation we have solved Maxwell equations numerically using the 2D-FDTD method with grid size

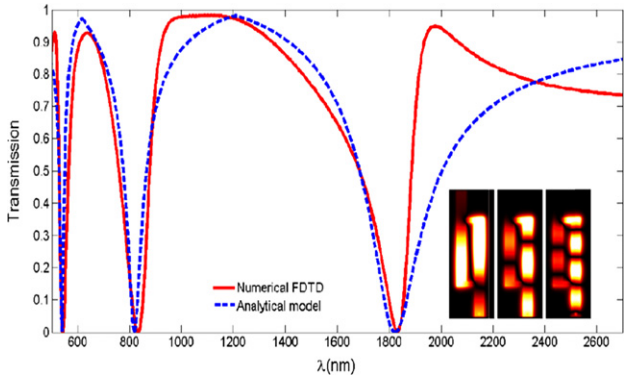

Figure 6. The transmission spectra of a filter with parameters of $W_H = 40$ nm, $W_V = 100$ nm, $L_x = 200$ nm, and $L_y = 500$ nm using analytical and numerical methods. The inset shows the field distribution in Hz for the first three resonance wavelengths, from left to right: first, second and third resonance wavelength.

2 nm × 2 nm [35]. Absorption of the field components approaching the boundaries of the spatial grids is guaranteed by implementation of convolutional perfectly matched layers (CPML). To calculate the transmission spectra, two lines at points of P_{In} and P_{Out}, shown in figure 1, are set to detect the power. P_{In} denotes the incident power, P_{Out} presents the transmitted power and the transmission is calculated by $T = P_{Out}/P_{In}$. The transmission spectra for a filter with parameters of $W_H = 40$ nm, $W_V = 100$ nm, $L_H = 200$ nm, $L_V = 500$ nm and $d = 100$ nm are shown in figure 6 from using both analytical and numerical methods. Although, due to using a simplified model, there are deviations between the analytical and numerical results, it is seen that both results show the same behavior. The stable standing waves excited in the ring are shown in figure 6 for the first three resonance wavelengths.

Next, we study the effect of the internal parameters of the structure on the transmission spectra. It will be shown that the analytic model can be used to explain the effect of changing the internal parameters of the structure on the transmission spectra as well. One influential parameter is $L = L_V + L_H$, which is half the average perimeter of the ring. To study the influence of L, we change only the value of L_V while L_H is set as 200 nm. In figure 7(a), transmission spectra are shown for three structures with different values of L using the FDTD method, while in figure 7(b) the first three resonance wavelengths are shown versus different values of L and compared with the results obtained from the analytic model. It is seen that the results obtained using the analytical model agree reasonably with the simulation results. Based on figure 7(b), the resonance wavelengths have a linear relation with L, thus the resonance wavelengths can be easily adjusted by changing the value of L. Here the effect of the asymmetry caused by the difference between L_H and L_V on the performance of the structure as a filter is also studied, because by setting $L_H = 200$ and changing L_V in fact we are increasing the asymmetry of the structure. As can be seen from figure 7(a), the effect of changing L_V mostly results in shifting the resonance wavelengths and has no considerable effect on the bandwidth of the structure or the performance of the structure as a filter. Increasing L, as

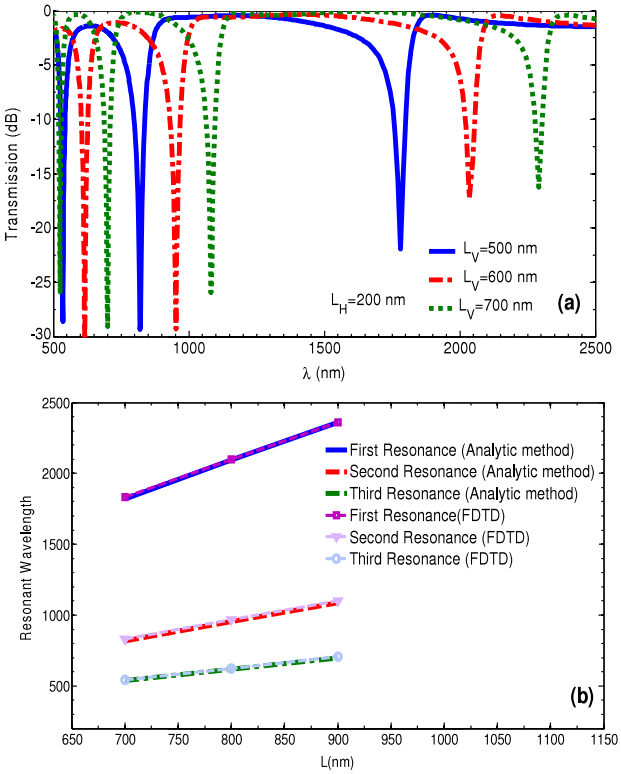

Figure 7. (a) The transmission spectra of the rectangular band-stop filter for three structures with different values of L. (b) The first three resonance wavelengths for different values of L, comparing results obtained by FDTD with the analytical model.

well as shifting the resonance wavelengths, has a small effect on the extinction ratios of the resonance wavelengths. As is demonstrated in figure 7(a), the extinction ratios of the first resonance wavelengths for three corresponding structures with $L_V = 500$ nm, 600 nm, 700 nm are 23 dB, 17 dB, 16 dB respectively.

Another parameter is the effect of the difference between W_H and W_V on the transmission spectra. For this purpose W_H varies while W_V is set to be 100 nm and the other parameters are fixed as $L_x = 200$ nm and $L_y = 500$ nm. The transmission spectra for four corresponding structures with different W_H using the FDTD method are shown in figure 8(a). It is observed that, on increasing the parameter W_H or decreasing the gap between W_H and W_V, the resonance wavelengths show a blue shift and the bandwidth and extinction ratio of transmission spectra decrease. The quality factors (defined as $Q = \lambda/\Delta\lambda$, where λ is the resonance wavelength of the ring and $\Delta\lambda$ is the full-width at half-maximum of transmission spectra) at the first resonance wavelength for four corresponding structures with $W_H = 30$ nm, 40 nm, 50 nm and 60 nm are 5.5, 10.5, 30.5 and 48.5 respectively. The extinction ratio for these corresponding structures is 27 dB, 23 dB, 15 dB and 12 dB respectively. One can see from figure 8(b) that the transmission spectra using the analytical model predicts the same behavior observed in the FDTD results. As can be seen, the effect of the gap between W_H and W_V on the bandwidth of the transmission spectra is more than the effect of the difference between L_x and L_y.

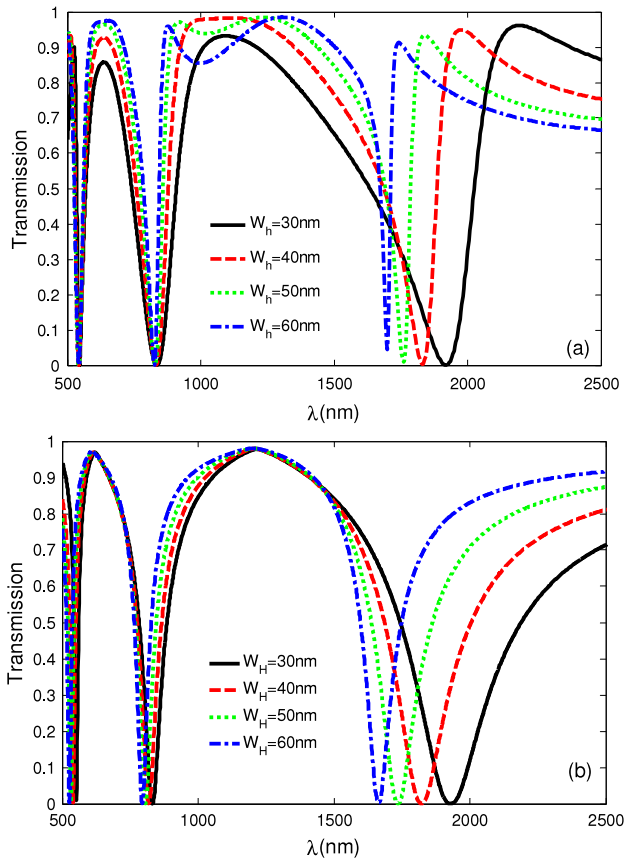

Figure 8. The transmission spectra of the rectangular band-stop filter for four structures with different values of W_H by using (a) the numerical FDTD method and (b) the analytical model.

Based on figure 8, the bandwidth of the spectra can easily be controlled by adjusting the gap between W_H and W_V.

To use this filter for CWDM standard channels, the bandwidth of the spectra should be 20 nm. By setting the parameters of the structure as $W_V = 100$ nm, $W_H = 80$ nm, the filter can be used for CWDM standard channels. Here we used the structure to filter the three CWDM channels with central wavelengths $\lambda_1 = 1291$ nm, $\lambda_2 = 1311$ nm, $\lambda_3 = 1331$ nm. The quality factors at these wavelengths are 65, 66 and 67 respectively. It is shown in figure 9 that by changing L the central wavelength can be controlled, so by choosing an appropriate L the filter can be used for other CWDM channels as well.

5. Conclusion

A band-stop filter based on a plasmonic nanowaveguide with an asymmetric rectangular ring is proposed and analyzed numerically, and the results are verified using an analytical model based on transmission line. It is shown that the analytical model is good for calculating the resonance wavelengths, explaining the behavior of the filter, and studying the effects of changing the internal parameters of the filter on the transmission spectra. It is demonstrated that the resonance wavelengths can be adjusted by manipulating the perimeter of the ring. It is shown the bandwidths of the

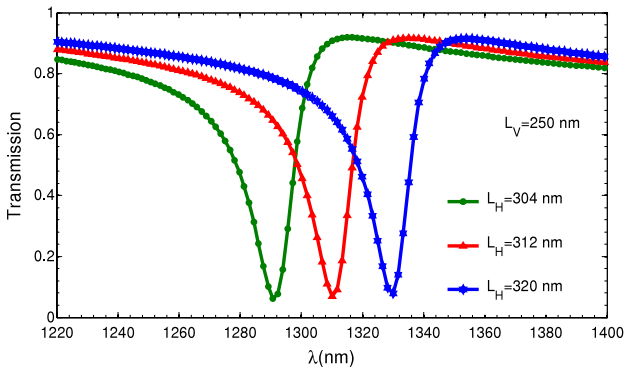

Figure 9. The transmission spectra of band-stop filters used for CWDM channels.

resonance spectra can be controlled by changing the gap between the widths of horizontal and vertical waveguides used in the ring and by adjusting the gap we use the filter for CWDM standard channels.

References

[1] Maier S A, Kik P G, Atwater H A, Meltzer S, Harel E, Koel B E and Requicha A A G 2003 Local detection of electromagnetic energy transport below the diffraction limit in metal nanoparticle plasmon waveguides *Nature Mater.* **2** 229–32

[2] Barnes W L, Dereux A and Ebbesen T W 2003 Surface plasmon subwavelength optics *Nature* **424** 824–30

[3] Luo X G and Yan L S 2012 Surface plasmon polaritons and its applications *IEEE Photon. J.* **4** 590–5

[4] Tanaka K, Tanaka M and Sugiyama T 2005 Simulation of practical nanometric optical circuits based on surface plasmon polariton gap waveguides *Opt. Express* **13** 256–66

[5] Liu L, Han Z and He S 2005 Novel surface plasmon waveguide for high integration *Opt. Express* **13** 6645–50

[6] Chen P, Liang R, Huang Q, Yu Z and Xu X 2011 Plasmonic filters and optical directional couplers based on wide metal–insulator–metal structure *Opt. Express* **19** 7633–9

[7] Veronis G and Fan S 2005 Bends and splitters in metal–dielectric–metal subwavelength plasmonic waveguides *Appl. Phys. Lett.* **87** 131102

[8] Guo Y H, Yan L S, Pan W, Luo B, Wen K H, Guo Z, Li H Y and Luo X G 2011 A plasmonic splitter based on slot cavity *Opt. Express* **19** 13831–8

[9] Wang B and Wang G P 2004 Surface plasmon polariton propagation in nanoscale metal gap waveguides *Opt. Lett.* **29** 1992–4

[10] Bozhevolnyi S I, Volkov V S, Devaux E, Laluet J-Y and Ebbesen T W 2006 Channel plasmon subwavelength waveguide components including interferometers and ring resonators *Nature* **440** 508–11

[11] Wang T B, Wen X W, Yin C P and Wang H Z 2009 The transmission characteristics of surface plasmon polaritons in ring resonator *Opt. Express* **17** 24096–101

[12] Setayesh A, Mirnaziry S R and Abrishamian M S 2011 Numerical investigation of tunable band-pass\band-stop plasmonic filters with hollow-core circular ring resonator *J. Opt. Soc. Korea* **15** 82–9

[13] Hosseini A and Masoud Y 2007 Nanoscale surface plasmon based resonator using rectangular geometry *Appl. Phys. Lett.* **90** 181102

[14] Zand I, Mahigir A, Pakizeh T and Abrishamian M S 2012 Selective-mode optical nanofilters based on with stub

structures plasmonic complementary split-ring resonators *Opt. Express* **20** 7516–25
[15] Setayesh A, Mirnaziry S R and Abrishamian M S 2011 Numerical investigation of a tunable band-pass plasmonic filter with a hollow-core ring resonator *J. Opt.* **13** 035004
[16] Guo Y H, Yan L S, Pan W, Luo B, Wen K H, Guo Z and Luo X G 2012 Characteristics of plasmonic filters with a notch located along rectangular resonators *Plasmonics* 1–5
[17] Lu H, Liu X M, Mao D, Wang L R and Gong Y K 2010 Tunable band-pass plasmonic waveguide filters with nanodisk resonators *Opt. Express* **18** 17922–7
[18] Hu F, Yi H and Zhou Z 2011 Band-pass plasmonic slot filter with band selection and spectrally splitting capabilities *Opt. Express* **19** 4848–55
[19] Lee P H and Lan Y C 2010 Plasmonic waveguide filters based on tunneling and cavity effects *Plasmonics* **5** 417–22
[20] Tao J, Huang X G and Zhu J H 2010 A wavelength demultiplexing structure based on metal-dielectric–metalplasmonic nano-capillary resonators *Opt. Express* **18** 11111–6
[21] Matsuzaki Y, Okamoto T, Haraguchi M, Fukui M and Nakagaki M 2008 Characteristics of gap plasmon waveguide with stub structures *Opt. Express* **16** 16314–25
[22] Lin X S and Huang X G 2008 Tooth-shaped plasmonic waveguide filters with nanometeric sizes *Opt. Lett.* **33** 2874–6
[23] Tao J, Huang X, Lin X, Chen J, Zhang Q and Jin X 2010 Systematical research on characteristics of double-sided teeth-shaped nanoplasmonic waveguide filters *J. Opt. Soc. Am.* B **27** 323–7
[24] Liu J, Fang G, Zhao H, Zhang Y and Liu S 2009 Surface plasmon reflector based on serial stub structure *Opt. Express* **17** 20134–9
[25] Pannipitiya A, Rukhlenko I D and Premaratne M 2011 Analytical modeling of resonant cavities for plasmonic slot-waveguide junctions *IEEE Photon. J.* **3** 220–33
[26] Pannipitiya A, Rukhlenko I D and Premaratne M 2010 Improved transmission model for metal-dielectric-metal plasmonic waveguides with stub structure *Opt. Express* **18** 6191–204
[27] Tao J, Huang X G, Lin X, Zhang Q and Jin X 2009 A narrow-band subwavelength plasmonic waveguide filter with asymmetrical multiple-teeth-shaped structure *Opt. Express* **17** 13989–94
[28] Han Z H, Forsberg E and He S 2007 Surface plasmon Bragg gratings formed in metal–insulator–metal waveguides *IEEE Photon. Technol. Lett.* **19** 91–3
[29] Cheng W, Abbas M N, Chang Z C, Shih M H, Wang C M, Wu M C and Chang Y C 2011 Angle-independent plasmonic infrared band-stop reflective filter based on the $Ag/SiO_2/Ag$ T-shaped array *Opt. Lett.* **36** 1440–2
[30] Han Z, Van V, Herman W N and Ho P T 2009 Aperture-coupled MIM plasmonic ring resonators with sub-diffraction modal volumes *Opt. Express* **17** 12678–84
[31] Hu F and Zhou Z 2011 Wavelength filtering and demultiplexing structure based on aperture-coupled plasmonic slot cavities *J. Opt. Soc. Am.* B **28** 2518–23
[32] Maier S A 2007 *Plasmonics: Fundamentals and Applications* (Berlin: Springer)
[33] Kocabas S E, Veronis G, Miller D A B and Fan S 2008 Transmission line and equivalent circuit models for plasmonic waveguide components *IEEE J. Sel. Top. Quantum Electron.* **14** 1462–72
[34] Veronis G, Kocabas S E, Miller D A B and Fan S 2009 Modeling of plasmonic waveguide components and networks *J. Comput. Theor. Nanosci.* **6** 1808–26
[35] Taflove A and Hagness S C 2005 *Computational Electrodynamics: The Finite-Difference Time-Domain Method* (Norwood, MA: Artech House)